Polymer 261 (2022) 125420

Contents lists available at ScienceDirect

Polymer

journal homepage: www.elsevier.com/locate/polymer

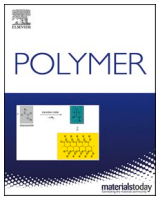

Fracture performance of epoxy foam: Low density to bulk polymer

George Irven [a,b], Declan Carolan [a,b], Alexander Fergusson [a,b], John P. Dear [b,*]

[a] FAC Technology, 53 Lydden Grove, London, SW18 4LW, UK
[b] Department of Mechanical Engineering, Imperial College London, London, SW7 2AZ, UK

ARTICLE INFO

Keywords:
Epoxy foam
Fracture toughness
Fracture energy
Density
Fractography

ABSTRACT

Epoxy foams with densities ranging from 180 to 500 kg/m^3 were prepared and mechanically tested in compression, tension, and single-edge notched bending (SENB) configurations. Fracture results revealed a marked transition in behaviour at a critical density, between 227 kg/m^3 and 249 kg/m^3. Lower density foams failed at low SENB displacement, producing low toughness and fracture energy results, whereas higher density foams failed at higher SENB displacements, with correspondingly higher values of toughness and fracture energy. The stress-intensity factor increased monotonically with density, from 0.1 to 0.79 MPa m$^{1/2}$. The fracture energy, G_{Ic}, of the foams reached values of up to 3.5 times that of the bulk polymer, 268 J/m^2. Lower density foams below the transition in fracture behaviour exhibited a small number of large cells, caused by cell coalescence, and a wider cell size distribution than the denser foams. This distribution appears linked to the transition in fracture behaviour. The behaviour revealed in this paper raises the point whether in future design criteria, where foams are now often used in composite sandwich structures, allowance should be made for denser foams to be used as appreciable increases in fracture energy of the foam core are achievable.

1. Introduction

Structural polymer foams are often used as core materials for composite sandwich structures. The combination of high specific strength, corrosion resistance and low radar signature makes composite sandwich structures an attractive structural choice for many disciplines [1]. Plantema [2], Allen [3], and Zenkert [4] have summarised the literature, theory, and practical aspects of sandwich structures. The theory surrounding the failure of sandwich beams is well understood, Gibson and Ashby [1] developed a series of failure maps for a beam in bending. However, composite sandwich structures have been shown to be particularly susceptible to point load and impact damage [5]. In these cases, the brittle nature of composite materials can lead to substantial overdesign of sandwich structure components, counteracting their weight and cost savings benefits. The damage resistance of a composite sandwich structure, which is a critical parameter for it to withstand damage, can be improved by improving the toughness of the individual components. Previous research by this group has demonstrated that by altering the layup of the individual plies in the composite skins, a significant increase in impact resistance of the structure can be obtained [6,7]. More recently, impact performance of sandwich structures has been improved through toughening the matrix of the sandwich skin [8]. During the impact testing of the epoxy-foam-core sandwich structures in the previous research, extensive cracking within the core was found. Fracture toughness of core materials is important, core cracking often leads to cracks propagating parallel to the skin leading to delamination of the skins from the core [9]. As such, this project builds on previous research and details a systematic study of the effect of density on the fracture performance of epoxy foams. The aim of the project is to discover how the fracture properties change from low density foam though to the bulk material. This range will include materials that are better described as voided solids.

Gibson and Ashby [1] provide an extensive study of foam material mechanical properties and propose micromechanical models thereof. Only these models will be compared to the experimental data within this research for simplicity. There are numerous other models available covered by Mills [9], however, these models are for specific cell geometries and are often very complex. Modulus, strength and fracture toughness will be compared to the models with a focus on fracture toughness and how this relates to fracture energy. Currently, no models exist for predicting the fracture energy of cellular solids. Toughness is a crucial property for foams as in tension they fail by the propagation of a single crack [1]. Marsavina [10] presents a summary specifically of micromechanical models for foam fracture. The models relate the

* Corresponding author.
E-mail address: j.dear@imperial.ac.uk (J.P. Dear).

https://doi.org/10.1016/j.polymer.2022.125420
Received 5 September 2022; Received in revised form 9 October 2022; Accepted 11 October 2022
Available online 14 October 2022

fracture toughness of the foam to the fracture strength of the bulk material, the relative density, and various lengths such as cell size and edge thickness. Marsavina and Linul [11] recently conducted a comprehensive review of the fracture toughness of rigid polymeric foams. They conclude that linear elastic fracture mechanics (LEFM) can be applied rigid polymer foams. Furthermore, fracture toughness does not, within reason, depend on the size or shape of specimens.

With regard to conducting fracture tests on polymer foams over a range of densities, early work was conducted by McIntyre and Anderton [12] on polyurethane foams. They found a linear relationship between K_{Ic} and density below 200 kg/m^3, however, the relationship became non-linear beyond this density. When G_{Ic} was calculated from these toughness values, interesting transitions were observed as modulus varied with density at a different rate to K_{Ic}. Zenkert and Bäcklund [13] conducted tests on polyvinyl chloride foam of nominal density 200 kg/m^3 and found that the fracture toughness decreased slightly with increasing mean cell diameter. They also confirmed that the difference between linear elastic fracture mechanics and non-linear analyses were small such that K_{Ic} and G_{Ic} could be used. Viana and Carlsson [14] tested a range of polyvinyl chloride foams from 36 to 400 kg/m^3 though a different grade of foam was used for the densest foam. They found a linear relationship between K_{Ic} and density up to 300 kg/m^3. However, the 400 kg/m^3 foam falls considerably below this relationship. They also found a minimum specimen thickness of 12.8 mm was required before further increases in thickness had no effect. Bureau and Kumar [15] investigated the fracture toughness of microcellular polycarbonate foam with relative density between 0.7 and 0.9. They found that while the fracture toughness of the 0.7 relative density foam was reduced compared to the bulk polymer, the fracture energy was increased due to a reduction in modulus.

Few studies exist on the effects of density on the mechanical properties of chemically blown epoxy foam. Stefani et al. [16] conducted compression tests on fifteen chemically blown epoxy foams from 200 to 550 kg/m^3. The modulus and strength of the tested foams follow power law relationships as observed in this research. The results are lower than those measured here, most likely due to differences in the foaming resin giving different bulk material properties. Wang et al. [17] manufactured epoxy foam using expandable microspheres from 450 to 1000 kg/m^3. Once again, the modulus and strength follow power law relationships. In fact, the densest foam in the current research matches precisely with the lower end of the results obtained by Wang et al. [17]. More recently, epoxy foams have been manufactured in small 50 ml batches via a mechanical whipping process by Jalalian et al. [18]. The compressive strengths achieved are consistent with the current research. The modulus is much lower, this could be due to the high proportion of non-curing surfactant or the 10 mm height of the compression samples. The machined top and bottom surfaces on thin compression samples result in a high ratio of broken cells causing a low measured modulus.

2. Materials

A commercially sensitive epoxy based foaming resin formed the basis of the materials investigated in the current work. Eight foams with varying densities from 183 to 506 kg/m^3 were manufactured. The resin mixture was kept constant while the amount of blowing agent was varied between 0.25 and 2.00 parts per hundred resin (PHR) in 0.25 PHR increments. Foams will be referred to within this research by the amount of blowing agent used in their manufacture. Epoxy foams were manufactured by mixing a stoichiometric amount of hardener into the foaming resin mixture with the blowing agent. The mixture was then poured into a rectangular mould and cured at 21 °C for 24 h, followed by a 24 h post-cure at 40 °C. The long cure cycle at a precisely controlled temperature is required when manufacturing foams as the viscosity, particularly the thixotropic response, of the foam is critical to developing and maintaining an optimal microstructure at each density. Bulk epoxy plates were manufactured from a resin formulation that closely matches that of the foaming resin. This resin was first degassed in a vacuum. A stoichiometric amount of the curing agent was then added, mixed, and degassed again. Bulk polymer panels were cast by pouring the resin mixture into aluminium moulds to produce either 3 mm, 8 mm, or 14 mm thick plates from which bulk specimen test samples could be machined.

3. Methods

Of both the foams and bulk epoxy plates, single-edge notched bending (SENB) tests in three-point bend configuration were conducted to determine the fracture energy, G_{Ic}, and fracture toughness, K_{Ic}, in accordance with ASTM D-5045 [19]. Multiple studies have confirmed the SENB specimen to be suitable for fracture toughness testing in foam [14,20]. In order to satisfy the plane strain condition, foam test specimens were machined with dimensions 140 mm × 28 mm × 14 mm. Bulk epoxy specimens were 80 mm × 16 mm x 8 mm. Foam specimens were pre-notched to a depth of 10 mm before being cut to a depth of 14 mm with a razor blade held in a custom device that was fixed to a drill press, allowing a consistent notch depth to be achieved. Razor blades are frequently used in the literature to create cracks in foam fracture toughness specimens [13,21–24]. The foams are morphologically transversely isotropic with respect to the foam rise direction. Morphological anisotropy is known to induce anisotropy in the mechanical and fracture properties of foams [25,26]. The cracks in the foams in this research propagate in the foam rise direction. Furthermore, all mechanical testing is carried out in the foam rise direction. Bulk epoxy specimens were pre-notched to a depth of 6 mm before subsequent tapping of the notch to produce a sharp crack to a depth of ≈8 mm using a chilled razor blade. Testing was conducted using a screw-driven universal testing machine at a constant crosshead displacement rate of 1 mm/min. The fracture toughness was calculated via:

$$K_{Ic} = \frac{P}{bw^{½}} f\left(\frac{a}{w}\right) \tag{1}$$

where P is the load at failure, b and w are the sample thickness and width, respectively, and $f(a/w)$ is a fitting function depending on the crack length, a. The fracture energy, G_{Ic} was calculated using the energy method via:

$$G_{Ic} = \frac{U}{bw\varphi} \tag{2}$$

Where U is the energy under the corrected load-displacement curve and φ is an energy calibration factor as defined in the ASTM standard [19]. At least five replicate specimens were tested for each formulation.

The compressive properties of the epoxy foams were tested according to ASTM D1621 [27] using a screw-driven universal testing machine. Samples with dimensions of 30 mm × 30 mm x 30 mm cubes were cut from foam panels with a diamond saw. These samples were tested in the foam rise direction. The samples were placed between stainless steel testing platens, and a load was then applied with a crosshead displacement rate of 2 mm/min. Compressive yield strength was calculated from the maximum stress within a strain of 10% as defined in the ASTM standard [27]. Some of the foams did not exhibit a distinct yield point within the initial 10% strain. As a result, a 0.2% offset yield strength was also calculated to better enable the comparison of the results with existing models. The compression samples were also used to calculate density. The samples were measured and weighed with an electronic balance. Measuring multiple samples allowed for variations in density across a foam panel to be monitored.

Tensile tests of the epoxy foams were carried out on dog bone samples bonded between two metallic load blocks as displayed in Fig. 1. The load blocks were connected to a test machine via pins. A load was then applied with a crosshead rate of 0.5 mm/min. These samples were orientated in the foam rise direction. The tensile failure stress of the

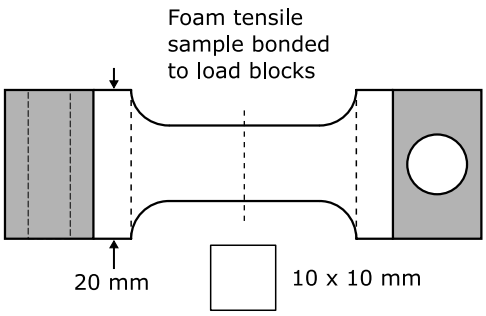

Fig. 1. Schematic of foam tensile samples.

epoxy foams was measured. The foam samples were sprayed with a black speckle and photographs were taken at 2 s intervals throughout the test with a digital single-lens reflex camera. GOM Correlate [28] digital image correlation software was then used to calculate strain both parallel and perpendicular to the test direction.

Tensile tests of the bulk epoxy were conducted to determine the uniaxial tensile stress versus strain curves in accordance with ISO-527 [29]. Dumbbell specimens with a gauge length of 30 mm were machined directly from 3 mm cast plates. The tests were carried out at a constant crosshead displacement rate of 1 mm/min. A clip-gauge extensometer was utilised to directly measure the strain in the test specimen. At least five replicate tests were carried out.

Compression tests of the bulk epoxy were conducted to determine the uniaxial compressive stress versus strain curves in accordance with ASTM D695 [30]. Prismatic samples 14 mm × 14 mm x 28 mm were used. Grease and a self-orienting platen were used to ensure accurate results. The tests were carried out at a constant crosshead displacement rate of 1 mm/min.

Imaging of both polished and fractured foam samples was conducted using a Tescan Mira scanning electron microscope (SEM). Polished samples were prepared using a standard wet grinding technique up to 2000 grit sandpaper. Imaging of the polished foam samples revealed valuable information regarding the morphology and microstructure of the foams. ImageJ image processing software was used to analyse the SEM images of the polished foam. Fig. 2 displays an example of two SEM images and their respective processed images using the ImageJ software. Cells were manually drawn around using either the freehand or circle tools within the software. Measurements of these elements could then be taken such as area, aspect ratio and angle of maximum diameter. At least 220 cells were measured for each foam.

4. Results

4.1. Microscopy: polished samples

Each foam sample was cut and polished to give a smooth surface to image using an SEM. Example SEM images of foams 0.25–1.00 PHR blowing agent are exhibited in Fig. 3 while images of foams 1.25–2.00 PHR blowing agent are displayed in Fig. 4. The foam rise direction is from the bottom of images to the top. The characteristic length of the cells of all the foams are plotted in a cumulative distribution plot in Fig. 5. The characteristic length is calculated as four times the area over the perimeter, $4A/P$, which is simply the diameter for a cell appearing circular. The ImageJ software determines the cell aspect ratio by first fitting an ellipse to each cell. The aspect ratio is then calculated as the ratio of the major and minor axis of the fitted ellipse. A box plot of cell aspect ratio is plotted in Fig. 6. A box plot of the cell areas for each foam is plotted in Fig. 7. The blue rectangle on the box plots contains the median as a red line and the first quartile either side as the edges of the box. The whiskers extend to the last data point with a value within 1.5 times the interquartile range from the edge of the box. Red dots are data points that fall outside of the whiskers and are considered outliers. Data for each foam including the density and relative density is displayed in Table 1. The foam in this research is foamed by a chemical blowing agent within the resin. As bubbles nucleate, they initially manifest as spheres such as the cells found in Fig. 3 (a). The bubbles that finally formed these cells lacked any interaction between neighbouring cells due to sufficient space and therefore remained as spheres until the foam cured. The additional bubbles formed due to the increased addition of blowing agent begin to run out of space to grow without interacting with

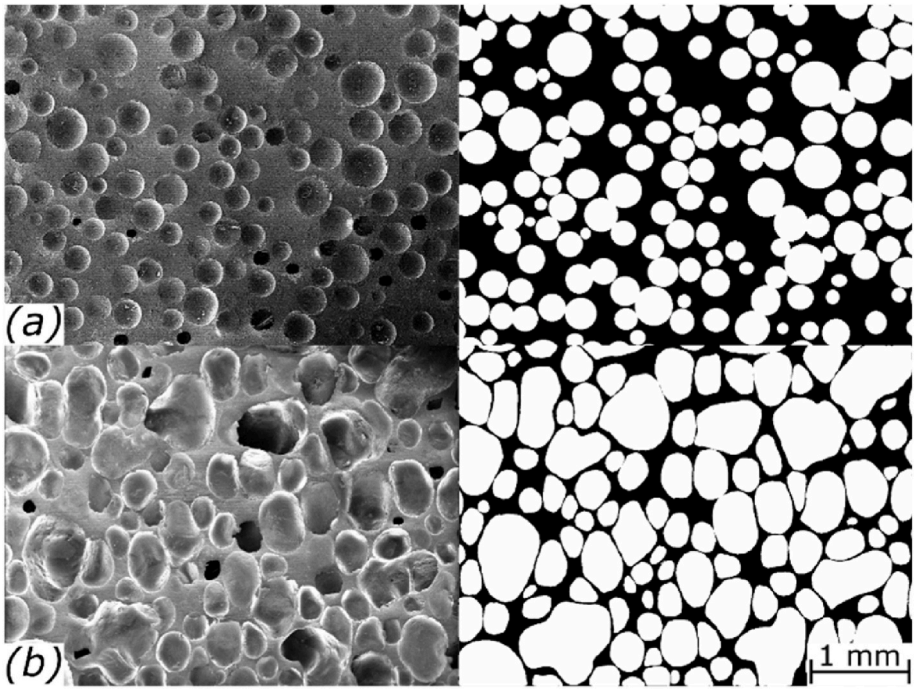

Fig. 2. Examples of SEM images and their respective processed images. (a): 0.25 PHR blowing agent – high density foam and (b): 2.00 PHR blowing agent – low density foam.

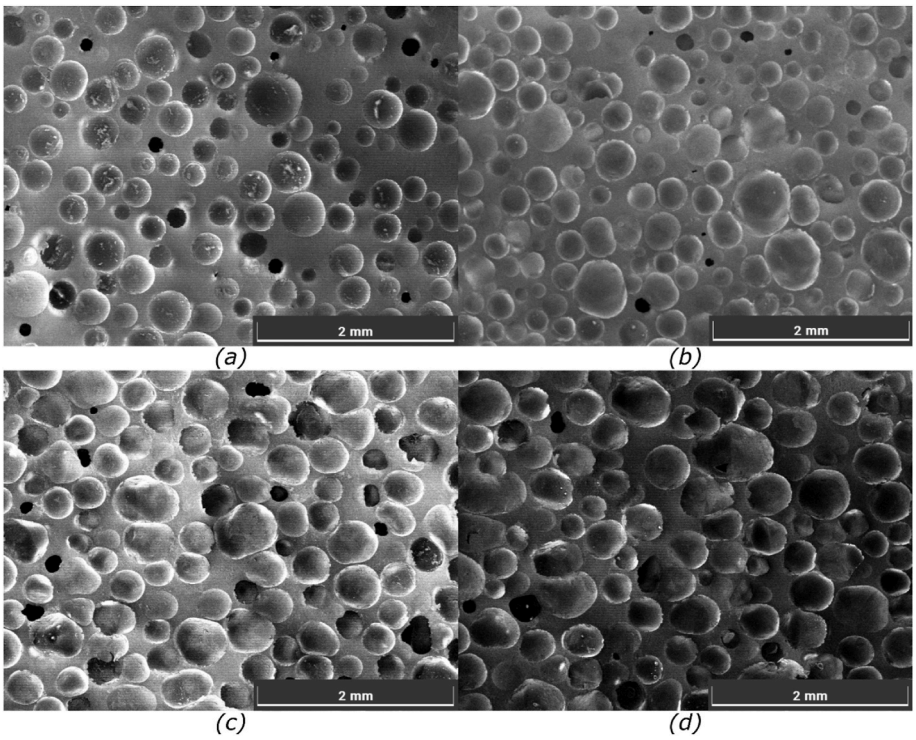

Fig. 3. SEM micrographs of polished foam samples. (a): 0.25 (b): 0.50 (c): 0.75 (d): 1.00 PHR of blowing agent.

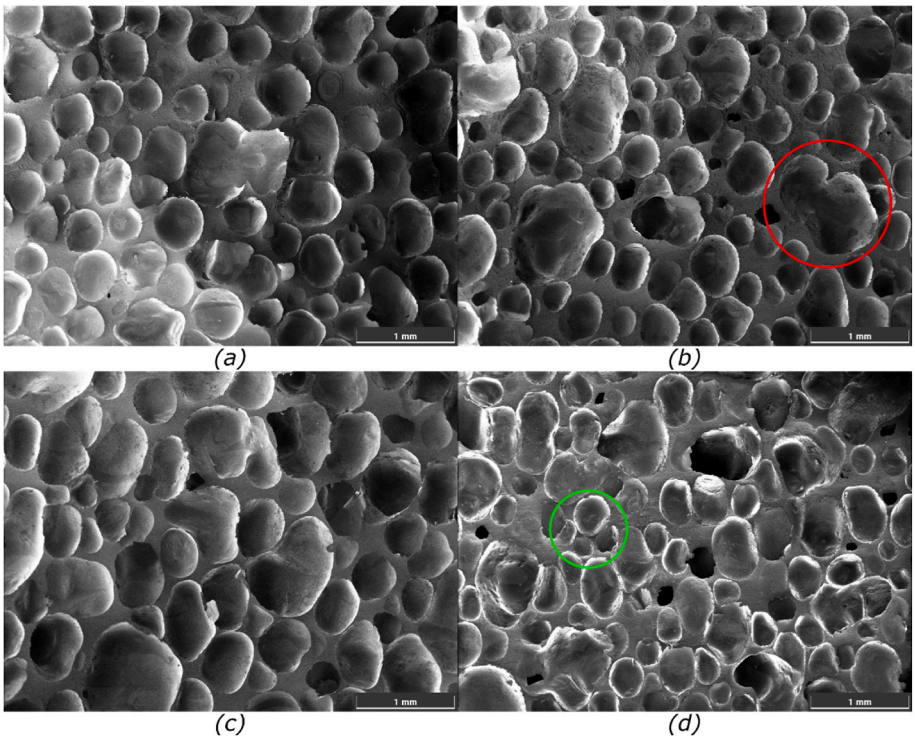

Fig. 4. SEM micrographs of polished foam samples. (a): 1.25 (b): 1.50 (c): 1.75 (d): 2.00 PHR of blowing agent. An example of cell coalescence is highlighted by a red circle. An example of small cells in close proximity is highlighted by a green circle. (For interpretation of the references to colour in this figure legend, the reader is referred to the Web version of this article.)

neighbouring bubbles. In fact, as the volume fraction of bubbles increases past 0.75 the bubbles necessarily deform each other [31]. A cell wall remains between these bubbles, and they begin to lose their spherical shape. Instead, they occupy the available space tending towards a polyhedral cell structure. This can be seen to happen as more blowing agent is added to the foams from Fig. 3 (a) through to Fig. 4 (d). It is interesting to note that the two densest foams, with bubble volume fractions well below 0.75, exhibit extremely similar cell size distributions in Fig. 5. The cells in these foams are spherical and rarely deform each other. The less dense of the two foams simply has more cells per

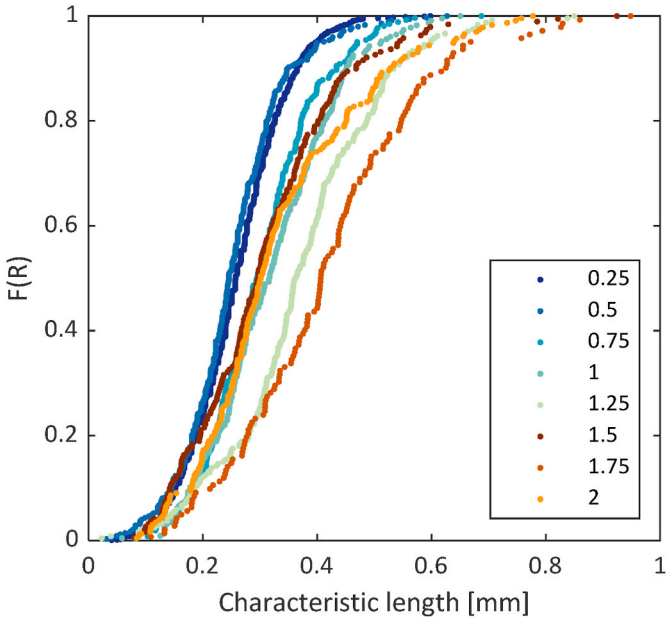

Fig. 5. Cumulative distribution plot of cell characteristic length for all of the foams with different amounts of blowing agent (0.25–2 PHR).

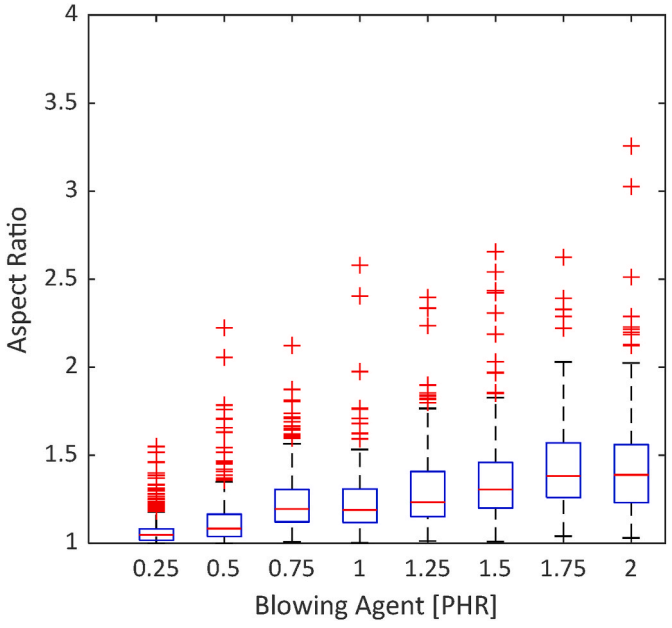

Fig. 6. Box plot of cell aspect ratio for each foam (at least 220 cells were measured for each foam and the blue rectangular box contains median as red line and first quartile either side). (For interpretation of the references to colour in this figure legend, the reader is referred to the Web version of this article.)

unit volume resulting in a lower density but very similar cells. The contrast between the cells in foams with the least and most blowing agent is clear in Fig. 2. It shows the cells in the 0.25 foam as circles whereas the cells in the 2.00 foam are not circles and have deformed against each other. Fig. 6 shows box plots of the aspect ratio of the cells of each foam. It is clear that the 0.25 and 0.5 foams have nearly perfectly spherical cells with aspect ratios very close to 1. As more blowing agent is added, the aspect ratio increases, and the cells become less spherical as they deform each other.

Two mechanisms that affect the lower density foams more significantly are drainage and cell wall rupture leading to coalescence [31].

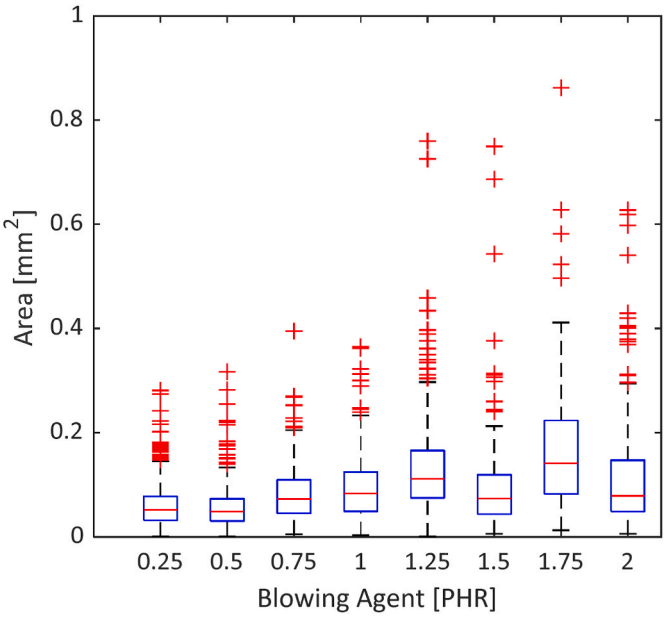

Fig. 7. Box plot of cell areas for each foam (at least 220 cells were measured for each foam and the blue rectangular box contains median as red line and first quartile either side). (For interpretation of the references to colour in this figure legend, the reader is referred to the Web version of this article.)

These mechanisms do not affect the higher density foams as the cell walls are much thicker and so are less susceptible to rupture even if some liquid drains away during foaming. Examples of cells that are likely to have been created by at least two smaller cells coalescing can be found across the images in Fig. 4, an example of this process has been circled in red in Fig. 4 (b). From Fig. 5, it can be seen that as more blowing agent is added to the foams the distribution of cell size shifts to ever larger values of characteristic length. However, all the foams still contain some small cells with characteristic lengths of approximately 0.1 mm. This is also clear in the box plots of the cell areas in Fig. 7. Fig. 7 also reveals that while the average size of cells increases as more blowing agent is added, this increase is not drastic. However, the box plots show that the foams with 1.25 PHR blowing agent and above have a small number of much larger cells. It is likely that these cells are formed by smaller cells coalescing.

The curves for the high-density foams in Fig. 5 are smoothly varying, however, the curves for foams 1.75 and 2.00 contain steps in the collected data. The steps are distinct increases in characteristic length and show increments in the number of cells that have coalesced to form the measured cell. Fig. 8 presents histograms of the angle of the maximum diameter of cells for foams 0.75–2.0. Foams 0.25 and 0.5 have not been included as the cells appear circular and so this data has very little meaning. The histograms show that low density foam cells are predominantly elongated in the foam rise direction. In contrast, higher density foams 0.75 and 1.0 have cells laying perpendicular to the foam rise direction. The increase in the relative mass of liquid in the denser foams above each bubble causes the foam to collapse very slightly prior to curing fully. All foams are transversely isotropic.

4.2. *Mechanical properties: strength and modulus*

The compressive strengths and moduli of the epoxy foams are presented in Table 1. Representative example stress versus strain curves for each of the foams is plotted in Fig. 9. Also shown are examples of how both yield strengths have been calculated. Yield strength of rigid cellular plastics is defined by the ASTM standard as the highest stress below a strain of 10% [27]. It is clear from Fig. 9 that the location of this yield strength changes as the density of the foam's changes. The lower density

Table 1
Density, Modulus, Strength and Fracture data for all foams with varying amounts of blowing agent (0.25–2.0 PHR).

Blowing Agent [PHR]	Density [kg/m^3]	Relative Density [−]	Compressive Yield Strength [MPa]	Compressive Modulus [MPa]	Tensile Strength [MPa]	Tensile Modulus [MPa]	Fracture Energy G_{Ic} [J/m^2]	Fracture Toughness K_{Ic} [MPa m$^{1/2}$]
Bulk	1169	1.00	109.3 ± 2.0	–	96.8 ± 0.7	3844 ± 84	268 ± 23	0.98 ± 0.06
0.25	506	0.43	17.34 ± 0.47	516 ± 23	14.23 ± 1.47	936 ± 133	931 ± 353	0.79 ± 0.12
0.50	367	0.31	9.19 ± 0.53	300 ± 15	6.75 ± 0.40	347 ± 56	917 ± 171	0.60 ± 0.04
0.75	310	0.27	6.15 ± 0.12	233 ± 9	4.88 ± 0.35	302 ± 112	821 ± 67	0.42 ± 0.01
1.00	292	0.25	5.44 ± 0.13	217 ± 4	3.90 ± 0.54	324 ± 35	831 ± 119	0.41 ± 0.02
1.25	249	0.21	4.11 ± 0.03	173 ± 3	2.50 ± 0.40	204 ± 26	625 ± 62	0.30 ± 0.01
1.50	227	0.19	3.34 ± 0.04	131 ± 4	2.11 ± 0.29	196 ± 19	102 ± 6	0.13 ± 0.01
1.75	201	0.17	2.84 ± 0.03	105 ± 10	1.83 ± 0.12	148 ± 38	76 ± 13	0.10 ± 0.01
2.00	183	0.16	2.33 ± 0.02	86 ± 1	1.67 ± 0.22	113 ± 24	82 ± 15	0.10 ± 0.01

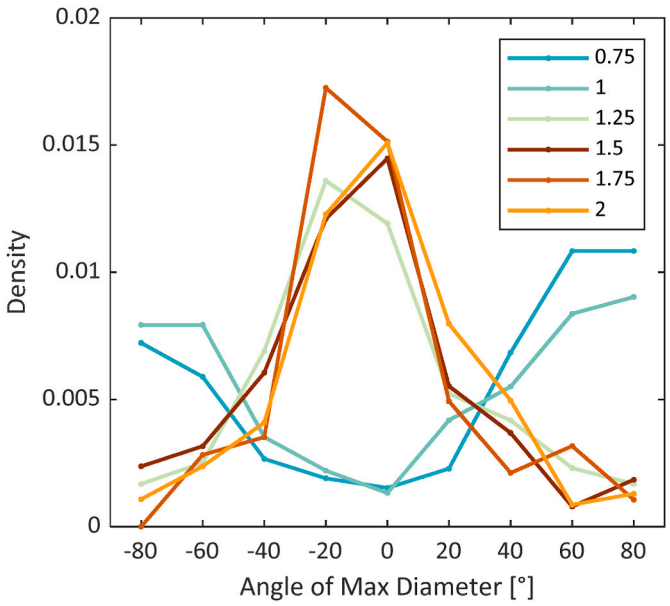

Fig. 8. Normalised Histogram of the angle of cell maximum diameter for foams 0.75–2.0 PHR blowing agent.

foams exhibit a distinct yield at approximately 5% strain after which the stress decreases before plateauing. On the other hand, the stress in the higher density foams either plateaus without such a distinct yield or continues to rise, such as with the highest density foam. In order to compare these results to models based on fundamental properties of foams, a 0.2% yield was also calculated for each foam. The ASTM yield strength for the 0.25 foam occurs at a point in the test with no significant change in response and so is unlikely to match with any model prediction. However, the 0.2% yield strength provides a value of strength just after the stress versus strain curve has deviated from an elastic response.

Gibson and Ashby [1] derived multiple models predicting the failure of foams in compression. These models were split into elastic collapse and plastic collapse. The elastic collapse models are not suited to structural foams such as the ones studied here. They were conceived to predict the plateau stress of elastomeric foams which recover fully from large strains. The plastic collapse models are based on a beam bending model and the formation of plastic hinges at the cell wall nodes. The plastic collapse models are split into an open cell and a closed cell model, shown in Equations (3) and (4), respectively, as:

$$\frac{\sigma^*_{pl}}{\sigma_{ys}} = C_1\left(\frac{\rho^*}{\rho_s}\right)^{3/2} \quad (open\ cell, \rho^*/\rho_s < 0.3) \tag{3}$$

$$\frac{\sigma^*_{pl}}{\sigma_{ys}} = C_2\left(\Phi\frac{\rho^*}{\rho_s}\right)^{3/2} + C_2'(1-\Phi)\left(\frac{\rho^*}{\rho_s}\right) \quad (closed\ cell, \rho^*/\rho_s < 0.3) \tag{4}$$

Where σ^*_{pl} is the plastic collapse stress of the foam, σ_{ys} is the yield strength of the bulk material, and ρ^* and ρ_s are the density of the foam and bulk material, respectively. For σ_{ys}, the bulk tensile yield strength is used as the model is based on beam bending. The constants, C_1, C_2, and C_2' are determined from fitting experimental data. For the closed cell model, Φ is a parameter which represents the amount of solid polymer in the cell edges over the amount of solid in the faces. This takes a value of unity for an open cell foam. Gibson and Ashby state the largest applicable relative density for these models is 0.3 [1]. Above this density the cell wall aspect ratio reduces such that the beam bending model used is

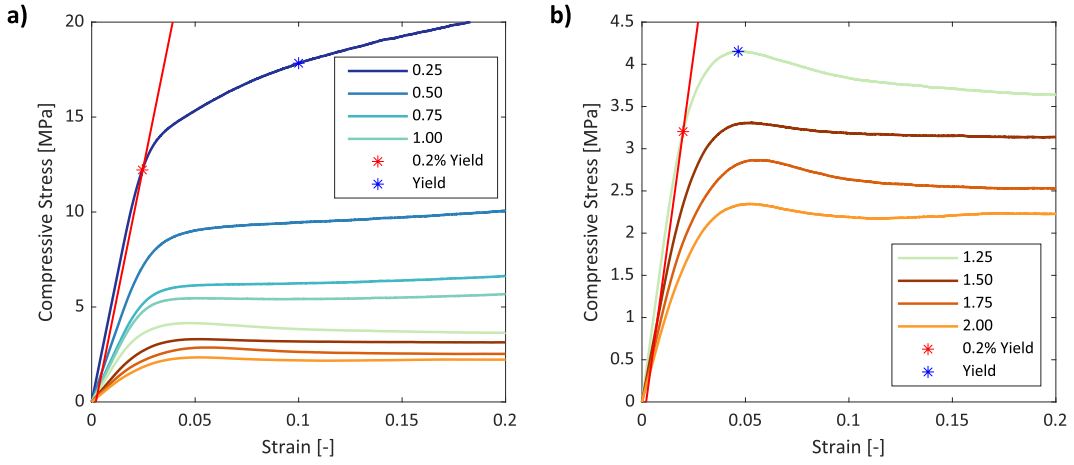

Fig. 9. Representative compressive stress versus strain for each foam and for the cases with 0.25 and 1.25 PHR blowing agent, the 0.2% Yield and ASTM Yield points are added.

no longer suitable and they yield axially in compression or tension. As a result, the models were fitted to the six foams below 0.3 relative density. Gibson and Ashby found that a value of 0.3 for C_1 in Equation (3) showed the best fit for the available data for open cell foams best. In addition, they found that the data for closed cell foams was also adequately described by the open cell Equation (3).

The values of compressive yield strength, σ^*_{YC}, compressive 0.2% yield strength, $\sigma^*_{0.2C}$, and tensile fracture strength, σ^*_{FT}, are plotted alongside two models in Fig. 10. This data is normalised against the tensile strength of the bulk polymer σ_{TS}. It is clear that as foam density increases the strength of the foam increases continuously. The values of tensile strength and 0.2% yield strength match very well. The line for Equation (3) with C_1 equal to 0.3 is plotted in Fig. 10. This model has some agreement with the 0.2% yield strength of the foams below 0.3 relative density. However, the best least squares agreement is between Equation (3) with C_1 equal to 0.44 and the ASTM yield strength. This line is also plotted in Fig. 10 and can be seen to agree very well with the data for foams below 0.3 relative density. It is understandable that not all sets of data are effectively fitted by these models using the same constants. One of the mains reasons for this is that the measured properties of the bulk polymer will not be the same as the properties of the bulk material that is contained within the foam. The bulk material in the foam will have a different molecular structure and will also contain by-products from the foaming reaction. This applies throughout this research where bulk material properties are used in models to predict or fit foam properties.

When considering the closed cell model in Equation (4), the least squares difference with the data below 0.3 relative density results in a value of unity for Φ which recovers the open cell model. The foams in this research are closed cell. However, similarly to the data available to Gibson and Ashby, they are adequately represented by the open cell Equation (3). In reality, the proportion of material in the cell edges, Φ, changes with density. As a result, a model which accurately represents a large range of foam densities would require a different exponent of the relative density term. In fact, the complete set of strengths in the current research is fit better by a relative density exponent of 2 as opposed to the 3/2 in Equations (3) and (4). This best fit is plotted in Fig. 10. The value of Φ in Equation (4) can be adjusted so that the model matches the experimentally measured strength at each individual density value. When this is done, the value decreases with density from 1 for the four least dense foams to 0.56 for the densest foam. This suggests that more material is found in the cell walls as the foam becomes denser. However, from Fig. 3 (a) and (b), it can be seen that the model of cell walls and edges is not appropriate, the foams are better represented by a solid containing voids. Hence, the previously mentioned limitations of these models to less than 0.3 relative density is reasonable.

Tensile modulus E^*_T and compressive modulus E^*_C are plotted in Fig. 11. The compressive modulus of the foam increases continuously as the density increases. The tensile modulus also increases in a similar manner. The elastic modulus of a foam in tension is the same as that in compression [1]. The data for the tensile modulus is of lower quality and has a larger uncertainty due to the correspondingly smaller cross section of the tensile tests compared to the compression tests. However, the tensile modulus is likely closer to the real modulus of the foam due to the DIC method of strain measurement. It was not possible to use DIC for the compression tests in the current research. There are significant difficulties with accurately measuring strain in a compressive test of structural foam as discussed in detail by Rajput et al. [32]. Primarily, parts of

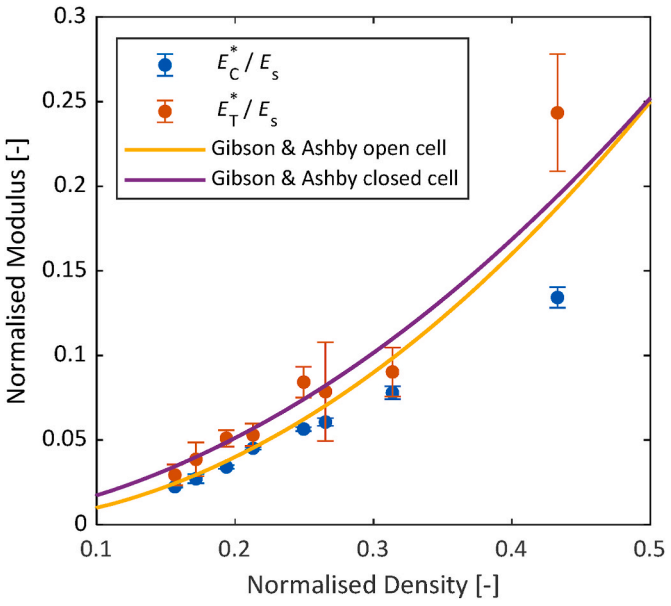

Fig. 11. *Normalised compressive and tensile modulus for all foams versus normalised density including both open cell and closed cell models* [1]. *(Normalised density of 0.16 corresponds to 2 PHR blowing agent and 0.43 corresponds to 0.25 blowing agent).*

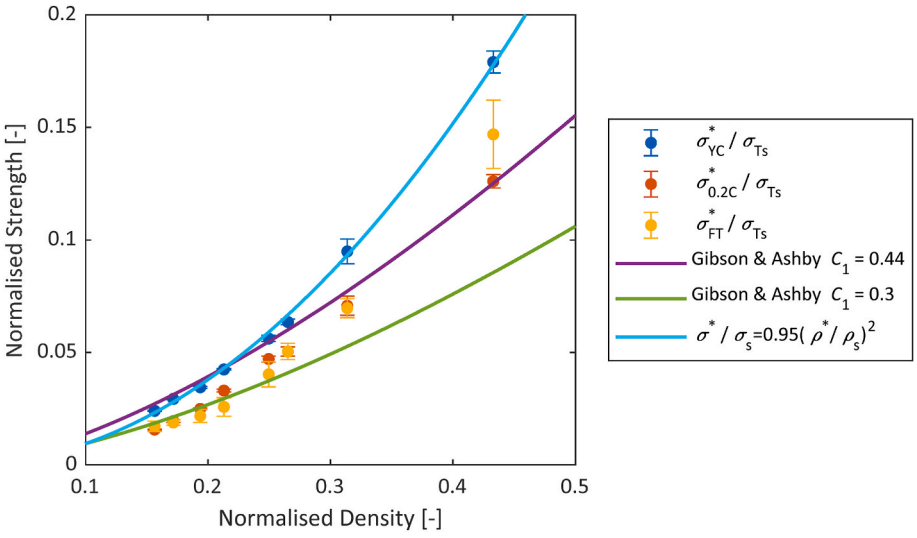

Fig. 10. *Normalised compressive and tensile strength of all foams versus normalised density including two models taken from Gibson and Ashby* [1] *(Normalised density of 0.16 corresponds to 2 PHR blowing agent and 0.43 corresponds to 0.25 blowing agent).*

the sample can begin to fail and form a crush band, as a result, the strain throughout the sample can vary massively. Furthermore, when a foam sample is machined the top and bottom layer of cells are broken and are therefore very compliant. Consequently, the measured modulus will both be lower than the true modulus and it will be sample size dependent. Nevertheless, the tensile and compressive moduli behave as expected with the tensile modulus being consistently higher.

Gibson and Ashby have also proposed models for predicting the modulus of both closed and open cell foam. These models are shown in Equations (5) and (6), respectively:

$$\frac{E^*}{E_s} = C_3\left(\frac{\rho^*}{\rho_s}\right)^2 \quad (open\ cell, all\ \rho^*/\rho_s) \tag{5}$$

$$\frac{E^*}{E_s} = C_4\Phi^2\left(\frac{\rho^*}{\rho_s}\right)^2 + C_4^{'}(1-\Phi)\left(\frac{\rho^*}{\rho_s}\right) \quad \left(closed\ cell\ \frac{\rho^*}{\rho_s} < 0.3\right) \tag{6}$$

where E^* and E_s are the modulus of the foam and the bulk polymer respectively. The constants C_3, C_4, and $C_4^{'}$ are determined from fitting experimental data. Gibson and Ashby found that the data for open cell foams was well fitted by taking C_3 as unity. They also found that data for closed cell foams was well fitted by taking C_4 and $C_4^{'}$ as unity also. It follows that the open cell model is valid through the full range of relative densities. The data in the current research also fits well with these constants as unity and so the models have been plotted as such in Fig. 11. The remaining constant to determine is Φ, the proportion of material within the cell edges. The modulus model was fitted over the full range of foam densities, therefore, the value for Φ is different to the one found for the strength model. A value of 0.9 best satisfies a least squares fit between Equation (6) and the tensile moduli of the foam in this work.

4.3. Fracture properties

SEM micrographs of the fracture surfaces of foam SENB samples are displayed in Figs. 12 and 13. Large areas of bulk material fracture are visible in Fig. 12 (a) compared to the other foams. It appears that the fracture surfaces show less bulk material than the polished samples. This is especially true when comparing the polished (Fig. 4) and fractured (Fig. 13) images of the low-density foams. During fracture a crack will take the path of least resistance, it then follows that this path will pass through the middle of large cells. As a result, the areas of bulk material seen on the polished samples of low-density foams are significantly smaller on the fracture surfaces of the same foams. On the other hand, the high-density foams which do not have any very large cells appear similar to the polished samples. There are no large cells to provide a significantly more favorable path that would reveal a difference between a polished and a fractured sample.

The fracture energy, G_{Ic}, and fracture toughness, K_{Ic}, of each foam and the bulk epoxy polymer are presented in Table 1. Representative load versus displacement graphs from SENB testing of each foam and the bulk epoxy polymer are plotted in Fig. 14. The foam samples have the same nominal dimensions, while the bulk sample load and displacement have been appropriately scaled, as if it had the same dimensions as the foam samples. When examining this plot, bear in mind that the crack lengths of each sample may vary slightly and that the plot is simply to demonstrate the varying responses of the samples. Furthermore, the 0.25 foam data has a particularly large spread and only one sample is plotted. For each sample, the load increases linearly as the displacement of the top roller of the three-point bend rig increases. The bulk epoxy polymer is the stiffest sample and also fails at the lowest displacement. The foams 1.5–2.0 fail in a catastrophic manner prior to 1 mm of displacement. There is then a dramatic change in response between foams 1.25 and 1.5. Foams 0.25–1.25 remain fully intact to a much larger displacement. Correspondingly there is a large increase in the measured fracture energy. The foam samples that fail at larger displacements show small dips in load which are quickly recovered. These dips suggest that small amounts of damage occurred within the sample, however, the foam withstood this damage without failing, i.e. the formation of a fracture process zone. These dips begin on the load versus displacement plot at approximately 0.75 mm. The foams that failed at lower displacements failed completely at a similar displacement suggesting they cannot withstand any microstructural damage without

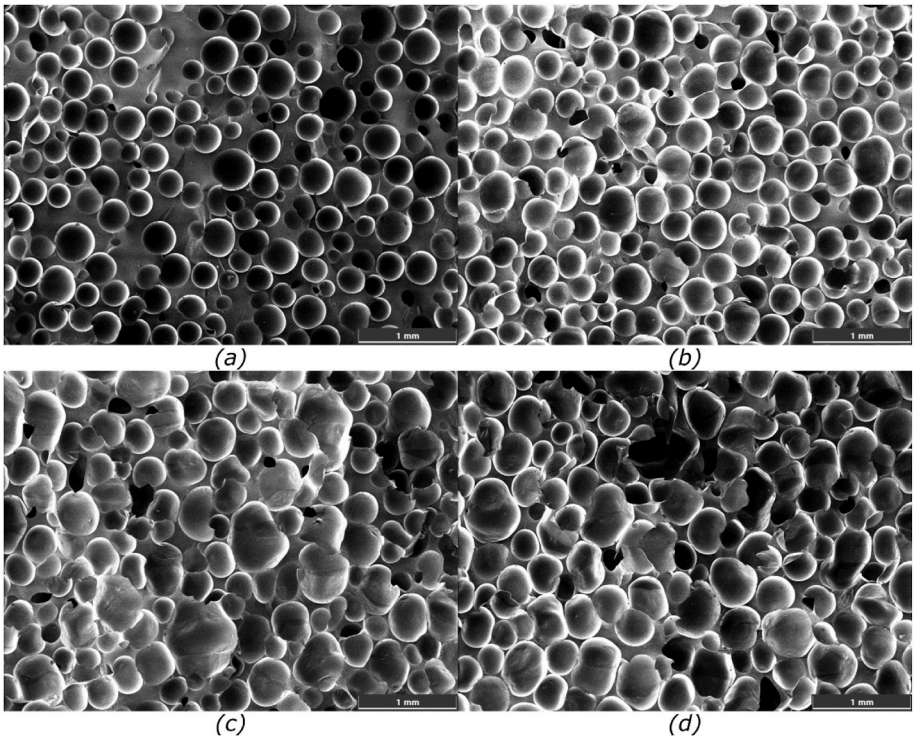

Fig. 12. SEM micrographs of the fracture surfaces of foam SENB samples. (a): 0.25 (b): 0.50 (c): 0.75 (d): 1.00 PHR of blowing agent.

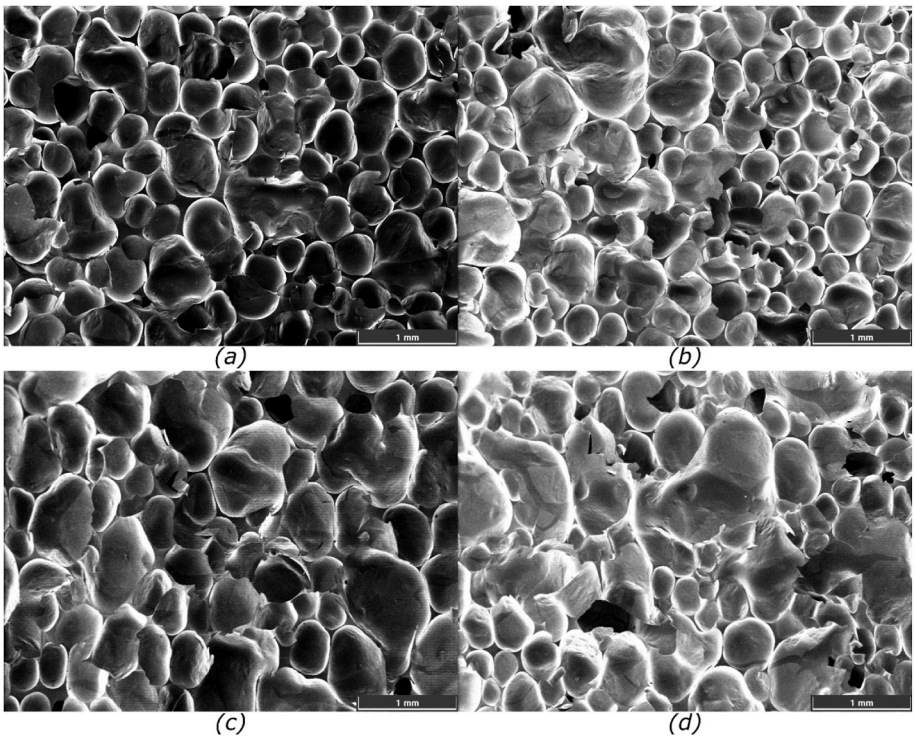

Fig. 13. SEM micrographs of the fracture surfaces of foam SENB samples. (a): 1.25 (b): 1.50 (c): 1.75 (d): 2.00 PHR blowing agent.

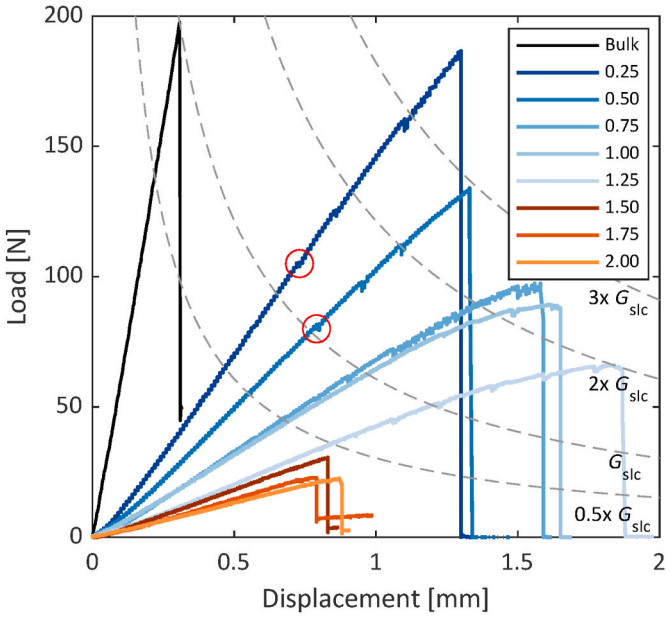

Fig. 14. Representative load versus displacement data from SENB testing. Lines of constant fracture energy are plotted as dashed lines. Examples of small load dips are circled in red. (For interpretation of the references to colour in this figure legend, the reader is referred to the Web version of this article.)

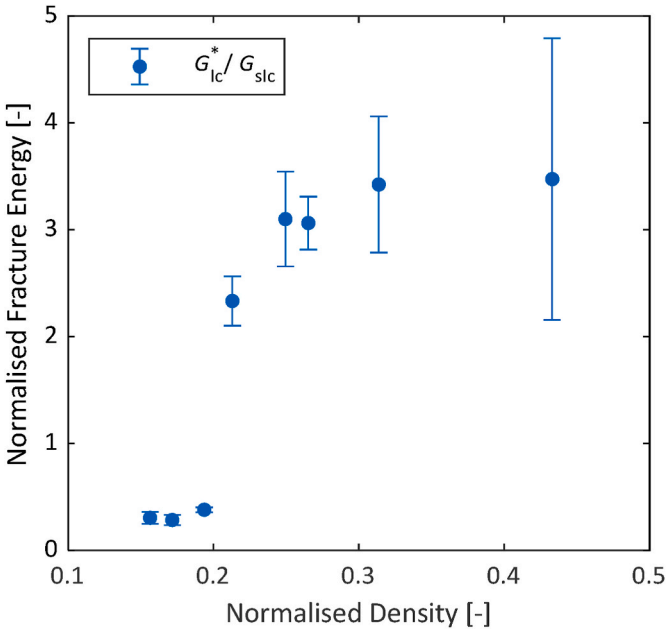

Fig. 15. Normalised fracture energy versus normalised density. (Normalised density of 0.16 corresponds to 2 PHR blowing agent and 0.43 corresponds to 0.25 blowing agent).

subsequently undergoing catastrophic failure.

The normalised fracture energy (epoxy foam fracture energy/bulk epoxy polymer fracture energy) versus normalised density is plotted in Fig. 15. The transition in fracture energy is clear. The first three foams have a similar normalised fracture energy of approximately 0.5. There is then a sudden increase to three followed by a plateau. Interestingly, the densest foam has a large spread of values. The size of the cells in both the 0.25 and 0.5 foams are similar, therefore, the inter-cell distance and the variance in inter-cell-distance in the 0.25 foam must be larger in order to achieve the higher density. Larger variation in inter-particle distance was found to be the main contributor to a larger variance in fracture strength of lower volume fraction syntactic foams by Carolan et al. [33]. Similar geometrically informed mechanisms are causing a large spread in fracture results here. The local density at the crack tip will determine whether the sample behaves like the bulk polymer or a foam. For example, the fracture surfaces of the foam shown in Fig. 12 (a) shows

large areas of bulk material. The results reflect this as some samples produced fracture energy values close to the bulk epoxy polymer while some other samples produced far higher fracture energies.

There is no simple explanation for the transition in fracture energy measured in this research. As discussed throughout this paper, the other measured mechanical properties of the foam increase continuously with density without significant increases between samples. The foams were all manufactured using the same methodology, using the same base resin. Furthermore, at each density, all samples for all tests were taken from a single foam panel. In fact, a preliminary study was conducted with a different base resin and a similar transition in toughness was found.

To further investigate the transition in fracture energy the fracture toughness of each sample was analysed. The normalised fracture toughness of each foam is plotted in Fig. 16. The two models plotted are based upon the model for foam fracture toughness first reported by Ashby [34] and then by Maiti [35] and Gibson and Ashby [1]. The model is shown in Equation (7):

$$K_{Ic}^{*} = C_5 \sigma_{ys} \sqrt{\pi l} \left(\frac{\rho^{*}}{\rho_s} \right)^{3/2} \tag{7}$$

where C_5 contains all the constants of proportionality which was found to be 0.65 when compared with the data available to Maiti et al. [35], and l is the cell size of the foam. This is the only model proposed by Gibson and Ashby that explicitly considers the cell size of the foam. The model is based upon calculating the stress in an equivalent linear-elastic continuum and comparing this to the fracture moment of an ideal cell. A cell size of 0.33 mm was used to plot and fit the models in Fig. 16. This is the average cell size measured from SEM images. Although this value is different for each foam it is raised to the power of a half and so its effect on the model output is limited. A value of 0.65 for C_5 provides a reasonable agreement with the fracture toughness's of the three least dense foams. However, the four foams after the transition in fracture energy are better fit by a value of unity for C_5. The densest foam then fits between the two models. The model predicts that a larger cell size will produce a higher fracture toughness. Curiously, the three least dense foams have a slightly larger cell size than the denser foams, this can be seen in Fig. 5. However, they have fracture toughness values less than the model values while the slightly smaller celled foams have higher fracture toughness values than the model values. The reason for this transitional behaviour is due to the cell size distribution. The less dense foams have larger cells on average and importantly also have a few very large cells. This distribution is clear from the box plots in Fig. 7 where the transition between having, or not having, some very large cells occurs at the 1.25 foam. The transition in fracture energy occurs just before the 1.25 foam as well. Another important consideration is that all the foams have small cells. In theory all these measured small cells could be due to the measuring plane cutting a larger cell at either of its poles. However, it is not possible for this to be the case if three small cells are found close together, as is often the case with the foams in this research. An example of this is highlighted in Fig. 4 (d). A foam having a large distribution of cell sizes will have a lower fracture toughness. Based on the Gibson and Ashby model of calculating the fracture moment of a cell edge, a foam containing smaller cells fails at a lower load. However, this model assumes that the cells along the crack front are the same size, and the load is equally distributed between each cell edge. A crack front containing small cells surrounded by larger cells will fail at a lower load as the larger cells are more compliant and are therefore carrying less load. As a result, the first failure in a foam with a wider cell size distribution will occur at a lower load and give a lower fracture toughness than a foam that has a tighter distribution of cell sizes. It follows that particularly large cells will exacerbate this problem if they are located along a crack front. A large cell will reduce the amount of cell edge material available to be loaded by reducing the local density at the crack tip. The cell edges of such a large cell would carry very little load due to the large compliance leading to premature failure of the cells either side of it. Furthermore, large cells result in a larger distance the crack can extend before it contacts the next cell. The result of this is that for the fracture model in Equation (7) to accurately predict experimental data it must also consider the distribution of cell sizes within the foam. Li et al. [36] conducted numerical analyses of the fracture toughness of low-density open-cell Voronoi foams. They found that as the disorder factor or randomness of the seed locations was increased, the fracture toughness was reduced. Although the cell size is not explicitly changed in this process, the foams with higher disorder factors will have a larger variation in the size of the cells.

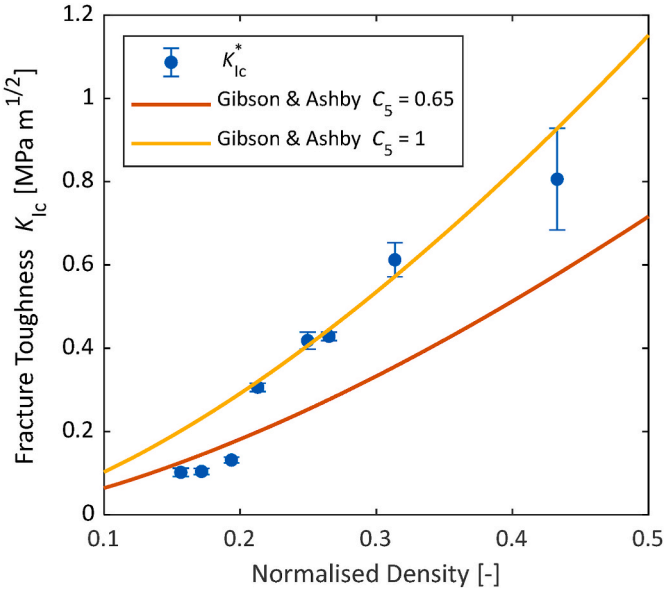

Fig. 16. *Normalised fracture toughness versus normalised density including two models* [1]. *(Normalised density of 0.16 corresponds to 2 PHR blowing agent and 0.43 corresponds to 0.25 blowing agent).*

No mention of the limits of applicability of this model were found in the literature. However, the upward curve of the model does not intercept the value of the bulk toughness of 0.98 MPa m$^{1/2}$. In fact, it predicts a value of 2.02 MPa m$^{1/2}$ with $C_5 = 0.65$ and $l = 0.33$ mm. In order to predict the true value, the cell size would need to be reduced to 0.077 mm. However, the cell size data collected in this study suggests that the cell size does not reduce as the relative density increases past 0.3. Instead, the number of cells simply decreases. This proposal is supported by research done by Wang et al. [37] who found cell size in chemically blown epoxy foam was approximately 0.3 mm diameter and unchanging between densities of 648–874 kg/m^3. The model proposed by Gibson and Ashby breaks down unless the crack front consists of foam cells with similar dimensions. In a material with a relative density of 0.4 such as the 0.25 foam, the crack front will begin to consist of significant proportions of solid material.

In order to find a fit for fracture toughness covering the full range of data in this research all of the normalised fracture toughness data points have been plotted in Fig. 17 (a). The fracture toughness of the 0.25 foam at a relative density of 0.43 is already approaching the toughness of the bulk polymer. As a result, any proposed fit must flatten out across the range of densities 0.4–1.0. Furthermore, the fit must pass through the origin and also increase sharply through the 0.2–0.4 relative density range. A sigmoid function can satisfy these requirements and fit the data well. The form of the proposed empirical fit is shown in Equation (8):

$$\frac{K_{Ic}^{*}}{K_{sIc}} = S\left(\frac{\rho^{*}}{\rho_s} \right) = K_{min} + \frac{(K_{max} - K_{min})}{\left(1 + 10^{m(\rho_{50} - \rho^{*}/\rho_s)}\right)} \tag{8}$$

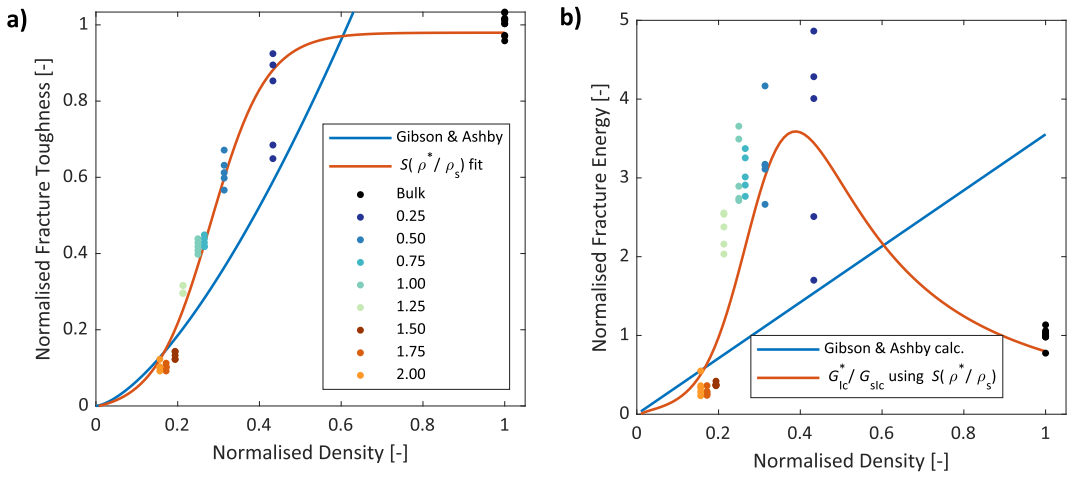

Fig. 17. *(a) Normalised fracture toughness versus normalised density including the Gibson and Ashby model [1] and a Sigmoid fit. (b) Normalised fracture energy versus normalised density including a calculated Gibson and Ashby line and fracture energy calculated from the Sigmoid fit of fracture toughness. (Data-points are colour coded, for the bulk polymer and the foams with different PHR blowing agent).* (For interpretation of the references to colour in this figure legend, the reader is referred to the Web version of this article.)

$$\frac{K^*_{Ic}}{K_{sIc}} = S\left(\frac{\rho^*}{\rho_s}\right) = -0.017 + \frac{(0.979 - (-0.017))}{\left(1 + 10^{6.3(0.28-\rho^*/\rho_s)}\right)} \tag{9}$$

Where K_{min} and K_{max} are the values which the function will tend to at $-\infty$ and $+\infty$ respectively and in this fit are close to 0 and 1. ρ_{50} is the normalised density value resulting in $(K_{max} + K_{min})/2$, and m is the gradient at this relative density value. This function was fit to all of the fracture toughness data with the additional requirement of passing through the origin. The resulting function is Equation (9). This function is plotted in Fig. 17 and shows very good fitting to the experimental data. It should be noted that this function is fitted to the fracture toughness data for the foams in one direction only. To completely characterise the foams fracture properties, another set of fracture tests would need to be performed perpendicular to the foam rise direction. Aside from providing a reasonable fit to the available experimental data, the choice of a sigmoid function seems physically rational as it is commonly used to provide physical context to percolating phenomena, e.g., in the design of electrically conductive polymers [38–40]. In these cases, the electrical percolation threshold is defined as the volume fraction of conductive material in the polymer that causes a sharp increase in the electrical conductivity of the material. More recently, He et al. [41] have hypothesised the concept of a structural percolation effect for the case of carbon fibres embedded within a syntactic foam matrix. They noted an initial loss in strength with a small volume fraction of included fibres, which thereafter recovered sharply to give improved behaviour of the composite. They argue that above a critical threshold of fibres the direct fibre to fibre stress functions as a percolated network whereas below this threshold, they act as individual particles. In the case of foams, it is the interactions between voids, which do not transmit any stress, that is important. At very high densities we have voids which are remote from each other. Thus, their impact on the fracture toughness remains low. Once the voids begin to get closer to each other they begin to interact and the sharp drop in fracture toughness is noted. In the lower (or foam) region, further decreases in density is not brought about by any of the individual voids becoming ever closer, but through void coalescence. Thus, no significant increase in stress interactions would be expected in this region.

It remained to be seen whether this fit for the fracture toughness would result in a calculated fracture energy fit that would agree with the experimental data. Fracture energy can be calculated from fracture toughness assuming a linear elastic response using Equation (10).

$$G_{Ic} = \left(1 - \nu^2\right) K^2_{Ic}/E \tag{10}$$

A suitable model for E has already been established in Equation (5). ν is Poisson's ratio which was found to be 0.33, in agreement with Gibson and Ashby [42]. It is noted that the elastic properties used in this equation were evaluated in the same principal direction as the fracture properties. Elastic properties may vary across the principal directions of the foam if there exists cell shape anisotropy such as in the low-density foams in this research. A G^*_{Ic} fit can be calculated by substituting Equation (9) and Equation (5) into Equation (10), this fit is plotted in Fig. 17 (b). The shape of the fit is a reasonable representation of the experimental data. Using the Gibson and Ashby K^*_{Ic} model in Equation (7) another G^*_{Ic} fit can be calculated. This results in a straight line due to the relative density powers used for each model cancelling out. It may seem plausible that a measure of energy per unit area such as fracture energy may increase linearly since the area of bulk material fractured within the foam increases linearly with relative density. However, this does not reflect the data in this study well. The data in this study is better fit using the sigmoid fit for fracture toughness in Fig. 17 (a) and the resulting fit for fracture energy in Fig. 17 (b).

This investigation has attempted to answer the question of how the fracture energy of a foam might vary with relative density. Consider the SENB load versus displacement curves in Fig. 14 and that the fracture energy is directly proportional to the area under these curves using Equation (2). Iso-fracture energy lines relative to the bulk polymer fracture energy are also plotted in Fig. 14. These iso-fracture energy lines are based on the nominal dimensions of the SENB samples in this research. The lines cover a range of sample compliances which can be achieved through varying the modulus or crack length of a sample. The crack lengths in this research are nominally the same. Therefore, in order to travel along the lines, the modulus of the sample must change. For example, if a foam sample had a lower modulus but the same fracture energy as the bulk polymer it would fail at a point on the G_{sIc} line with a higher displacement than the bulk polymer sample. It becomes clear why the foams with intermediate relative densities have fracture energies far greater than either the bulk material or very low-density foams. The maximum load does not fall proportionally with the extra displacement achieved by these high fracture energy foams. From Equation (10) we can see that if fracture toughness (proportional to the highest load achieved) falls at a slightly slower rate than modulus, the fracture energy of that material will increase. For example, in this research we have manufactured a foam with a normalised fracture toughness of 0.6, which has a normalised modulus of less than 0.1 and results in a normalised fracture energy over 3.

5. Conclusion

The variation in fracture energy of an epoxy foam has been studied as a function of the density of the foam. A critical foam density has been identified, above which the fracture energy is significantly higher than that of the base epoxy polymer. At densities lower than this, the fracture behaviour of the foam is consistent with the models proposed by Gibson and Ashby. The critical foam density for this epoxy polymer was identified as a relative density, ρ^*/ρ_s of 0.28. The tensile and compressive modulus and strength were found to be reasonably well described by Gibson and Ashby models across their recommended validity ranges. Notably, the transition from Gibson and Ashby behaviour to toughened behaviour occurs over a small density range. The data shows that the behaviour of the fracture toughness as a function of density, K_{Ic}^* is well described by a sigmoidal function over the entire density range, including the bulk polymer. The relative density of the transition in fracture properties coincides with changes in foam morphology observed by SEM. Lower density foams below the transition in fracture toughness displayed evidence of a few large cells and a wider cell size distribution. This wider cell size distribution appears to be the cause of the transition in fracture properties. Larger cell size distributions caused the premature failure of smaller cells at the crack front as larger cells are more compliant and do not carry a proportional amount of load. Larger cells also allow for cracks to propagate through low resistance paths within the foam. Interestingly, the tensile and compressive properties are not affected by cell morphology in the same way. It is proposed for applications where energy absorbing capabilities of the foam are critical, denser foams may be a more optimal choice, sacrificing a small gain in weight for a considerable gain in damage resilience.

CRediT authorship contribution statement

George Irven: Conceptualization, Methodology, Investigation, Formal analysis, Writing – original draft, Writing – review & editing. **Declan Carolan:** Conceptualization, Methodology, Formal analysis, Writing – review & editing, Supervision. **Alexander Fergusson:** Writing – review & editing, Supervision, Resources, Funding acquisition. **John P. Dear:** Writing – review & editing, Supervision, Funding acquisition.

Declaration of competing interest

The authors declare that they have no known competing financial interests or personal relationships that could have appeared to influence the work reported in this paper.

Data availability

Data will be made available on request.

Acknowledgements

George Irven would like to acknowledge an EPSRC faculty CASE PhD studentship with FAC Technology. [grant number EP/R513052/1].

Declan Carolan acknowledges the support of UKRI Future Leaders Fellowship. [grant number [MR/T023406/1]

References

[1] L.J. Gibson, M.F. Ashby, Cellular Solids, Cambridge University Press, 1997.
[2] F. Plantema, J. Sandwich Construction: the Bending and Buckling of Sandwich Beams, Plates and Shells, John Wiley and Sons Inc., New York, 1966.
[3] H.G. Allen, Analysis and Design of Structural Sandwich Panels, Pergamon Press, Oxford, 1969, https://doi.org/10.1016/C2013-0-02134-2.
[4] D. Zenkert, An Introduction to Sandwich Structures, EMAS, London, 1995.
[5] P.M. Schubel, J.J. Luo, I.M. Daniel, Impact and post impact behavior of composite sandwich panels, Composites Part A Appl Sci Manuf 38 (2007) 1051–1057, https://doi.org/10.1016/j.compositesa.2006.06.022.
[6] E. Rolfe, C. Kaboglu, R. Quinn, P.A. Hooper, H. Arora, J.P. Dear, High velocity impact and blast loading of composite sandwich panels with novel carbon and glass construction, J Dyn Behav Mater 4 (2018) 359–372, https://doi.org/10.1007/s40870-018-0163-5.
[7] E. Rolfe, R. Quinn, G. Irven, D. Brick, J.P. Dear, H. Arora, Underwater blast loading of partially submerged sandwich composite materials in relation to air blast loading response, Int. J. Light Mater. Manuf. 3 (2020) 387–402, https://doi.org/10.1016/j.ijlmm.2020.06.003.
[8] G. Irven, A. Duncan, A. Whitehouse, D. Carolan, A.D. Fergusson, J.P. Dear, Impact response of composite sandwich structures with toughened matrices, Mater. Des. 203 (2021), 109629, https://doi.org/10.1016/j.matdes.2021.109629.
[9] N.J. Mills, Polymer Foams Handbook: Engineering and Biomechanics Applications and Design Guide, Butterworth Heinemann, 2007.
[10] L. Marşavina, Fracture mechanics of cellular solids, in: CISM Int. Cent. Mech. Sci. Courses Lect., vol. 521, Springer, Vienna, 2010, pp. 1–46, https://doi.org/10.1007/978-3-7091-0297-8_1.
[11] L. Marşavina, E. Linul, Fracture toughness of rigid polymeric foams: a review, Fatig. Fract. Eng. Mater. Struct. 43 (2020) 2483–2514, https://doi.org/10.1111/ffe.13327.
[12] A. McIntyre, G.E. Anderton, Fracture properties of a rigid polyurethane foam over a range of densities, Polymer (Guildf) 20 (1979) 247–253, https://doi.org/10.1016/0032-3861(79)90229-5.
[13] D. Zenkert, J. Bäcklund, PVC sandwich core materials: mode I fracture toughness, Compos. Sci. Technol. 34 (1989) 225–242, https://doi.org/10.1016/0266-3538(89)90030-4.
[14] G.M. Viana, L.A. Carlsson, Mechanical properties and fracture characterization of cross-linked PVC foams, J. Sandw. Struct. Mater. 4 (2002) 99–113, https://doi.org/10.1177/1099636202004002227.
[15] M.N. Bureau, V. Kumar, Fracture toughness of high density polycarbonate microcellular foams, J. Cell. Plast. 42 (2006) 229–240, https://doi.org/10.1177/0021955X06063512.
[16] P.M. Stefani, A.T. Barchi, J. Sabugal, A. Vazquez, Characterization of epoxy foams, J. Appl. Polym. Sci. 90 (2003) 2992–2996, https://doi.org/10.1002/app.13006.
[17] L. Wang, X. Yang, J. Zhang, C. Zhang, L. He, The compressive properties of expandable microspheres/epoxy foams, Compos. B Eng. 56 (2014) 724–732, https://doi.org/10.1016/j.compositesb.2013.09.030.
[18] M. Jalalian, Q. Jiang, A. Bismarck, Air templated macroporous epoxy foams with silica particles as property-defining additive, ACS Appl. Polym. Mater. 1 (2019) 335–343, https://doi.org/10.1021/acsapm.8b00084.
[19] ASTM D5045-14, Standard Test Methods for Plane-Strain Fracture Toughness and Strain Energy Release Rate of Plastic Materials, American Society for Testing and Materials, West Conshohocken, USA, 2014, https://doi.org/10.1520/D5045-14 n.d.
[20] A. Pugna, R. Negrea, E. Linul, L. Marşavina, Is fracture toughness of pur foams a material property? Stat. Approach Mater. (Basel) 13 (2020) 1–13, https://doi.org/10.3390/ma13214868.
[21] T.C. Cotgreave, J.B. Shortall, The fracture toughness of reinforced polyurethane foam, J. Mater. Sci. 13 (1978) 722–730, https://doi.org/10.1007/BF00570506.
[22] M.J. Carling, Fracture Mechanics of Short Fibre Composites, Imperial College London, 1988.
[23] G.M. Viana, L.A. Carlsson, Influences of foam density and core thickness on debond toughness of sandwich specimens with PVC foam core, J. Sandw. Struct. Mater. 5 (2016) 103–118, https://doi.org/10.1177/1099636203005002020.
[24] E.E. Saenz, L.A. Carlsson, A.M. Karlsson, In situ analysis of fatigue crack propagation in polymer foams, Eng. Fract. Mech. 101 (2013) 23–32, https://doi.org/10.1016/j.engfracmech.2012.10.009.
[25] J. Andersons, J. Modniks, M. Kirpluks, U. Cabulis, The effect of cell shape anisotropy on fracture toughness of low-density brittle foams, Eng. Fract. Mech. 269 (2022), 108565, https://doi.org/10.1016/J.ENGFRACMECH.2022.108565.
[26] A.T. Huber, L.J. Gibson, Anisotropy of foams, J. Mater. Sci. 23 (1988) 3040.
[27] ASTM D1621-16, Standard Test Method for Compressive Properties of Rigid Cellular Plastics, American Society for Testing and Materials, West Conshohocken, USA, 2016, https://doi.org/10.1520/D1621-10.2 n.d.
[28] GOM correlate. https://www.gom.com/en/products/gom-suite/gom-correlate-pro. 2020.
[29] 527 -1 I, Plastics-Determination of Tensile Properties, International Organization for Standardization, Geneva, Switzerland, 2012 n.d.
[30] ASTM D695-15, Standard Test Method for Compressive Properties of Rigid Plastics, American Society for Testing and Materials, West Conshohocken, USA, 2015, https://doi.org/10.1520/D0695-15.2 n.d.
[31] P. Walstra, Principles of Foam Formation and Stability, Springer, London, 1989, https://doi.org/10.1007/978-1-4471-3807-5_1.
[32] M.S. Rajput, M. Burman, K\"{o}ll J, Hallstr\"{o}m S. Compression of structural foam materials – experimental and numerical assessment of test procedure and specimen size effects, J. Sandw. Struct. Mater. 21 (2019) 260–288, https://doi.org/10.1177/1099636217690500.
[33] D. Carolan, A. Mayall, J.P. Dear, A.D. Fergusson, Micromechanical modelling of syntactic foam, Compos. B Eng. 183 (2020), 107701, https://doi.org/10.1016/j.compositesb.2019.107701.
[34] M.F. Ashby, Mechanical properties of cellular solids, Metall. Trans. A, Phys. Metall. Mater. Sci. 14 (1983) 1755–1769, https://doi.org/10.1007/BF02645546. A.
[35] S.K. Maiti, M.F. Ashby, L.J. Gibson, Fracture toughness of brittle cellular solids, Scripta Metall. 18 (1984) 213–217, https://doi.org/10.1016/0036-9748(84)90510-6.

[36] J.E. Li, B.L. Wang, S.L. Guo, Numerical analysis of the fracture toughness of low-density open-cell Voronoi foams, Mech. Compos. Mater. 54 (2019) 789–798, https://doi.org/10.1007/S11029-019-9783-7/FIGURES/6.
[37] L. Wang, X. Yang, T. Jiang, C. Zhang, L. He, Cell morphology, bubbles migration, and flexural properties of non-uniform epoxy foams using chemical foaming agent, J. Appl. Polym. Sci. 131 (2014), https://doi.org/10.1002/app.41175 n/a-n/a.
[38] S. Kirkpatrick, The nature of percolation "channels, Solid State Commun. 12 (1973) 1279–1283, https://doi.org/10.1016/0038-1098(73)90865-X.
[39] S. Kirkpatrick, Percolation and conduction, Rev. Mod. Phys. 45 (1973) 574–588.
[40] J.K.W. Sandler, J.E. Kirk, I.A. Kinloch, M.S.P. Shaffer, A.H. Windle, Ultra-low electrical percolation threshold in carbon-nanotube-epoxy composites, Polymer (Guildf) 44 (2003) 5893–5899, https://doi.org/10.1016/S0032-3861(03)00539-1.
[41] S. He, D. Carolan, A.D. Fergusson, A.C. Taylor, Toughening epoxy syntactic foams with milled carbon fibres: mechanical properties and toughening mechanisms, Mater. Des. 169 (2019), 107654, https://doi.org/10.1016/j.matdes.2019.107654.
[42] L.J. Gibson, M.F. Ashby, Mechanics of three-dimensional cellular materials, Proc R Soc London, Ser A Math Phys Sci 382 (1982) 43–59, https://doi.org/10.1098/rspa.1982.0088.